ELSEVIER

Nuclear Instruments and Methods in Physics Research B 170 (2000) 245–258

NIM B
Beam Interactions with Materials & Atoms

www.elsevier.nl/locate/nimb

A computer code to simulate X-ray imaging techniques

Philippe Duvauchelle *, Nicolas Freud, Valérie Kaftandjian, Daniel Babot

Laboratoire de Contrôle Non Destructif par Rayonnements Ionisants (CNDRI), Institut National des Sciences Appliquées de Lyon, Bâtiment 303, 20 Avenue Albert Einstein, 69621 Villeurbanne Cedex, France

Received 23 March 2000

Abstract

A computer code was developed to simulate the operation of radiographic, radioscopic or tomographic devices. The simulation is based on ray-tracing techniques and on the X-ray attenuation law. The use of computer-aided drawing (CAD) models enables simulations to be carried out with complex three-dimensional (3D) objects and the geometry of every component of the imaging chain, from the source to the detector, can be defined. Geometric unsharpness, for example, can be easily taken into account, even in complex configurations. Automatic translations or rotations of the object can be performed to simulate radioscopic or tomographic image acquisition. Simulations can be carried out with monochromatic or polychromatic beam spectra. This feature enables, for example, the beam hardening phenomenon to be dealt with or dual energy imaging techniques to be studied. The simulation principle is completely deterministic and consequently the computed images present no photon noise. Nevertheless, the variance of the signal associated with each pixel of the detector can be determined, which enables contrast-to-noise ratio (CNR) maps to be computed, in order to predict quantitatively the detectability of defects in the inspected object. The CNR is a relevant indicator for optimizing the experimental parameters. This paper provides several examples of simulated images that illustrate some of the rich possibilities offered by our software. Depending on the simulation type, the computation time order of magnitude can vary from 0.1 s (simple radiographic projection) up to several hours (3D tomography) on a PC, with a 400 MHz microprocessor. Our simulation tool proves to be useful in developing new specific applications, in choosing the most suitable components when designing a new testing chain, and in saving time by reducing the number of experimental tests. © 2000 Elsevier Science B.V. All rights reserved.

Keywords: Non-destructive testing; Simulation; X-ray imaging; Quality control; Ray-tracing techniques; Computer-aided drawing; Contrast-to-noise ratio

1. Introduction

X-ray imaging techniques, such as radiography, radioscopy and tomography, are used in more and more diversified applications, notably in the medical field [1], materials science [2] and the food-processing industry [3]. For each specific

* Corresponding author. Tel.: +33-472-438213; fax: +33-472-438822.
E-mail address: philippe.duvauchelle@insa-lyon.fr (P. Duvauchelle).

0168-583X/00/$ - see front matter © 2000 Elsevier Science B.V. All rights reserved.
PII: S0168-583X(00)00185-3

application, it is generally a complex task to design the appropriate testing chain. A suitable X-ray emitter and detector have to be chosen, and the optimal parameter values (current and voltage of the X-ray tube, geometric adjustment, exposure time, etc.) have to be determined. To develop a new X-ray imaging system, or to optimize an existing one, long and expensive series of experimental tests and measurements are usually necessary. Sometimes the only method is to proceed by trial and error, and in practice, it is impossible to study exhaustively the influence of the many parameters that condition the final image quality. As a consequence, when the non-destructive testing (NDT) application is very delicate, the development stage may seem quite off-putting, or within the reach of specialists only.

To develop and optimize a new imaging system, and to master the influence of the various adjustable parameters, simulation can be a helpful tool. It offers powerful means for choosing the most suitable components and for predicting the future device performance, by acting as a virtual experimental bench. Simulated images, that can be obtained in little time and at low cost, may enable the behavior of the whole imaging system to be investigated in complex situations [4].

In that context, a four-year research program was initiated 18 months ago in the laboratory *Contrôle Non Destructif par Rayonnements Ionisants*, to model and simulate the functioning of any X- or γ-ray imaging chain, from the photon emission phenomena, up to the detector behavior, including the photon–matter interactions within any 3D object. During this first period, we started with photon attenuation in the object, and we laid emphasis on 3D geometric aspects.

This paper presents the basic principles we used and the possibilities offered by the computer code we developed. The algorithm is described in a schematic way and a few examples of simulated images are given. Finally, we introduce the contrast-to-noise ratio (CNR), which can be a very useful indicator for quantifying the detectability of defects in the inspected part. An example of a CNR map is presented and potential applications are briefly discussed.

2. Basic principles

Ray-tracing techniques, together with the X-ray attenuation law, are the basis of our computer code. From each source point, a set of rays is emitted towards every pixel center of the detector. Each ray may intersect a certain number of meshes on the sample surface or at the interfaces between different parts of the object (Fig. 1). The attenuation path length in every part of the object is calculated by determining the coordinates of all the intersection points. The photon number $N(E)$ that emerges from the sample and reaches a pixel of the detector is given by the attenuation law

$$N(E) = N_0(E)\Delta\Omega\prod_i \exp[-\mu_i(E)x_i] = N_0(E)\Delta\Omega\exp\left[\sum_i -\mu_i(E)x_i\right]. \quad (1)$$

In this formula, $N_0(E)$ refers to the number of photons with energy E, emitted by the source per solid angle unit; $\Delta\Omega$ is the solid angle that corresponds to the pixel, observed from the source point; $\mu_i(E)$ designates the linear attenuation coefficient associated with the material i at the energy E, and x_i the total path length through the material i. The solid angle $\Delta\Omega$ is given by the following equation:

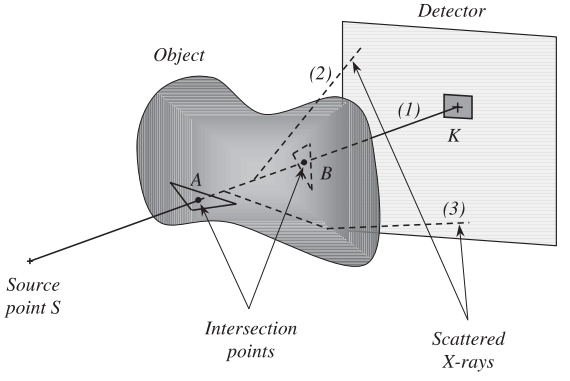

Fig. 1. Principle of the simulation. The ray SK intersects two meshes at points A and B. Geometrical calculations enable the attenuation path length AB to be determined. Ray (1): transmitted photons. Rays (2) and (3): scattered photons, not yet taken into account by our simulation code.

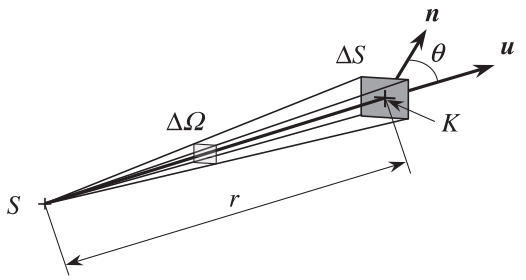

Fig. 2. The incident photon number, in the direction of any particular pixel, is proportional to the solid angle $\Delta\Omega$ associated with this pixel, seen from the source point S. The solid angle $\Delta\Omega$ can be calculated using Eq. (2).

$$\Delta\Omega \cong \frac{\Delta S \boldsymbol{n}\cdot\boldsymbol{u}}{SK^2} = \frac{\Delta S\cos\theta}{r^2}, \tag{2}$$

where ΔS stands for the pixel surface; $\theta = (\boldsymbol{n},\boldsymbol{u})$ refers to the angle between the pixel surface normal unit vector $\boldsymbol{n}$ and the unit vector $\boldsymbol{u}$ pointing from the source point S towards the pixel center K; r is the distance SK (Fig. 2). We assume that ΔS is small enough for the distance r to be considered as a constant for the whole pixel surface.

The image computed using Eq. (1) takes into account neither the contribution of the photons that are scattered within the object nor the scattering inside the detector, which is known to degrade spatial resolution. We did not take into account fluorescence and annihilation photons either. The Compton and Rayleigh scattering contributions to the image and the photon interactions with a real detector will be investigated in a future study. So far, we have simulated images with a "perfect" detector, in which every pixel is able to count all the photons that hit its surface.

3. Simulation possibilities

Our simulation software requires various input data and several databases to describe an experimental situation with maximum accuracy (Fig. 3). We first have to define the source characteristics: shape, size, position and orientation. To simulate geometric unsharpness, we have to divide the source area into elementary source points. Beam parameters enable, if need be, collimators to be taken into account. The geometry of the object, which may consist of several parts, possibly of different materials, is described with triangular meshes, using computer-aided drawing (CAD) software. Finally, the detector has to be defined (position, orientation, pixel number and size).

Besides the definition of geometric parameters, we have to choose a beam spectrum and the object material(s), which calls, respectively, for spectra and materials databases.

3.1. Source geometry

In experimental devices, if the γ- or X-ray emitter is small enough and the setup geometry chosen properly, the geometric unsharpness can be smaller than the pixel size, and therefore it can be neglected. To simulate such situations, the γ- or X-ray emitter can be modeled as a point source. Nevertheless, in practice, this ideal situation is quite rare and the unsharpness has to be taken into account because it leads to a degradation of the image spatial resolution and contrast.

To carry out realistic simulations, we chose a straightforward method, which consists in cutting the source area (considered as a flat surface in the first approach) into elementary source points, and repeating image computation with each of the latter. The number of source points as well as their spacing in the two directions are adjustable (Fig. 4). The source shape (rectangular, circular or elliptic) can also be chosen, to simulate different kinds of real emitters. For example, a cylinder-shaped radioactive source can be described as a rectangle, when it is seen from one side, or as a

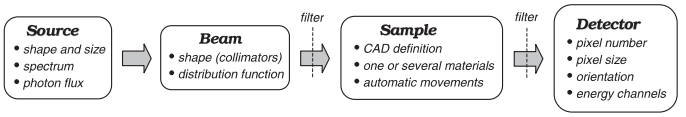

Fig. 3. Synoptic diagram of a simulated imaging chain. Every box in this figure corresponds to a section of the simulation software, in which several parameters are adjustable.

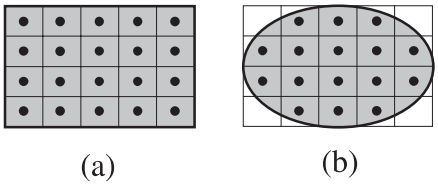

Fig. 4. The source shape can be chosen rectangular (a) or elliptic (b). Its size (length and width) and the numbers of elementary source points along the two axes are adjustable.

disk, if it is seen from the front. To illustrate the simulation of geometric unsharpness, three examples of simulated images, obtained with a tilted rectangular source divided into 150 elementary source points, are presented in Fig. 5. These examples show in particular that geometric unsharpness varies with the object position in the beam of the X-ray tube. If high precision is needed, a spatial distribution function can also be used to weight the elementary source points with an emission intensity coefficient. For example, in the case of a disk-shaped source, the central source points may be weighted with a higher coefficient than the source points located near the edge of the disk.

In short, simulation enables the influence of geometric unsharpness to be taken into account, even in complex situations. This can be useful in predicting the resulting spatial resolution degradation in any given X-ray imaging system, and in determining the best geometric adjustment (of the entire imaging chain: source–object–detector) to keep this degradation within acceptable limits.

3.2. Beam geometry

In experimental devices, collimators are sometimes required to limit the spatial extension of the incident beam. For example, in radiography or radioscopy setups, a collimator can be useful in diminishing the image degradation due to scattered photons, which constitute a parasitic signal in the image. In the medical field, it is also essential to keep the total dose absorbed by the patient as low as possible by exposing only the body part that has to be imaged. Some NDT techniques, such as Compton scattering or Rayleigh-to-Compton ratio measurements, also require very precise beam collimators that determine the measurement volume in the sample [5].

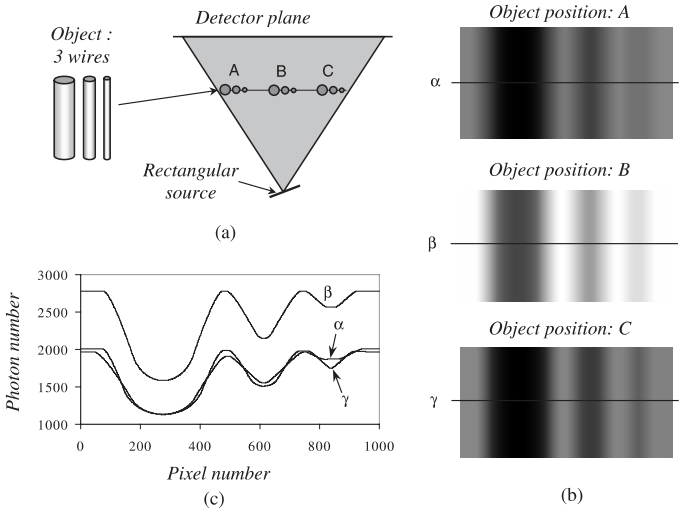

Fig. 5. Simulation of geometric unsharpness. (a) Three simulations were carried out with different positions of the object in the beam (labels *A* to *C*). (b) Region of interest of the simulated radiographs; when the object is moved towards the right, from *A* to *C*, the geometric unsharpness becomes lower, because the apparent size of the source decreases. (c) The profiles that correspond to lines α and γ show that the image quality is better in position *C* than in position *A*. The comparison with position *B* is more difficult: every pixel of the detector is seen from the source with a bigger solid angle than in position *A* and *C* and, therefore, the detector gets a higher photon number.

With a view to simulating photon scattering, we have integrated in our software the possibility of choosing the shape of the beam. The simplest model, when no collimator is used, is an isotropic beam. Quite obviously, this model is suitable for describing the emission of a radioactive source. It can also be used with X-ray tubes, provided that the space region where the object is located is small enough, in such a way that all the incident rays can be considered as equivalent, i.e., transporting the same photon flux. To describe the effect of different collimator types, a direction vector, corresponding to the central axis of the collimated beam, has to be defined. The beam cross-section shape (rectangular, circular or elliptic) and size have to be given too. Lastly, the rays that belong to the collimated beam can also be weighted by a distribution function, to take into account possible flux variations with the ray direction, due to both the X-ray tube and collimator characteristics.

3.3. Sample

3.3.1. Sample definition

To be able to carry out image simulations with a large variety of samples (mechanical parts, food industry products, biological samples, etc.), our computer code was designed to accept standard CAD files to describe the sample geometry. Many software packages enable complex 3D objects to be drawn and CAD files to be generated in a short time, for example, with the stereolithographic (STL) or unstructured cell data (UCD) format. These files contain a list of nodes and meshes (triangular facets) that fit the object surface. The precision of this fit, which is linked to the size of the meshes, can be adjusted.

The object may consist of different parts, possibly made of different materials, assumed to be homogeneous. The CAD model of each part can be handled independently. If a compound material is specified, the corresponding mass attenuation coefficient μ/ρ is calculated with the well-known formula

$$\mu/\rho = \sum_i \omega_i (\mu/\rho)_i, \tag{3}$$

where the index i refers to each element of the compound and ω_i stands for the fraction by weight associated to the element i.

3.3.2. Sample movements

To simulate the functioning of radioscopic or tomographic systems, it is necessary to carry out multiple simulation with automatic movements of the sample. These movements play the same role as stepper motors in experimental setups and they can be a combination of translations and rotations. For example, radioscopic image acquisition can be performed by means of a linear detector, with a translation of the sample, perpendicular to the plane constituted by the X-ray focal spot and the detector (Fig. 6).

Tomographic devices can be simulated as well, by computing all the projections that compose the sinogram. For example, we simulated several 2D tomographic experiments, with a cylindrical spatial resolution phantom, made of aluminum and with square holes 0.4–2.5 mm in width. A linear detector, composed of 500 pixels (0.2 mm wide), was used. We simulated several sinograms with different source sizes to assess the influence of geometric unsharpness on spatial resolution and to study the effect of the beam spectral distribution. An example of reconstructed tomographic slice, obtained with a point source and a polychromatic beam (100 kV X-ray tube voltage), is presented in Fig. 7. A more detailed study concerning the simulation of X-ray computed tomography has been carried out and examples of 3D imaging can be found in the corresponding publication [6].

3.4. Detector geometry

We took into account various parameters, such as the position and orientation in space of the detector plane, defined by the coordinates of the detector center and three rotation angles. This feature enables, for example, the influence of a poor geometric adjustment in an imaging chain to be studied (Fig. 8). By choosing the number and size of the pixels, the spatial resolution can be adjusted, but if a very high resolution is needed the

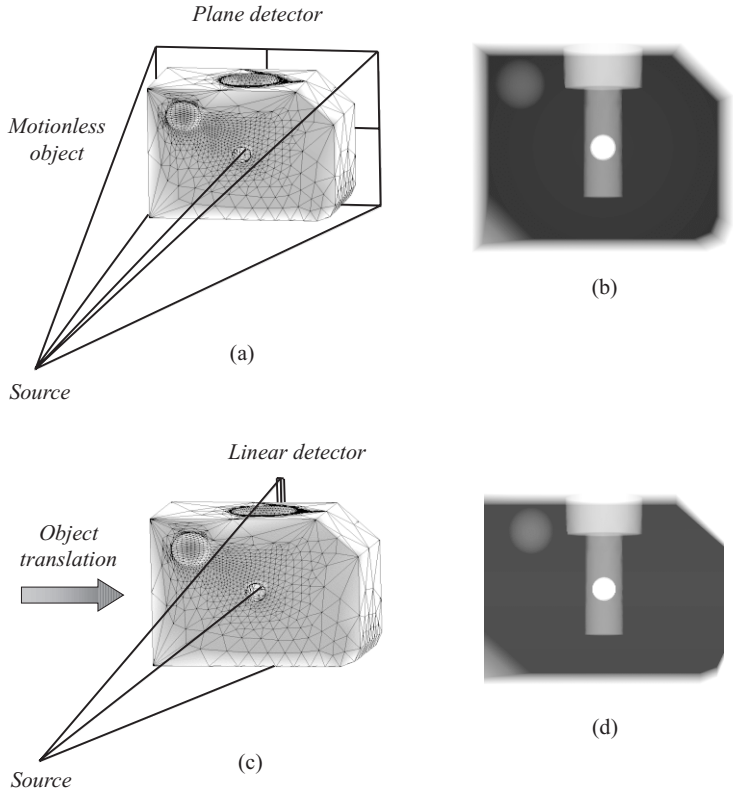

Fig. 6. (a) Schematic view of a radiography device, with a motionless object and a matrix detector. (b) Simulated radiograph with a detector composed of 360 × 280 pixels. The gray level gradation, at the edge of the object, is due to the beam divergence (the rays cut the sample edges slantwise). (c) Schematic view of a radioscopy system, with a horizontal translation of the sample and a linear detector. (d) Simulated radioscopy, obtained with 300 translation steps of the sample and a detector composed of 280 pixels. The two vertical edges of the object do not present any gradation as in the simulated radiography, because the rays that form the image do not diverge horizontally.

computation time may be long. To save computation time, only a region of interest of the object can be imaged.

Simulation based on ray-tracing techniques must be used with care because sampling is carried out when computing images. In a real detector, each pixel gives a signal corresponding to all the photons hitting its surface, whereas, in simulation, all the photons are "concentrated" in the center of the pixel. If this approximation is judged too rough, a finer computation can be performed by dividing each pixel into smaller sub-pixels. When the calculation is complete, the signals corresponding to the sub-pixels are just added to constitute the final signal (Fig. 9).

3.5. Energy spectrum

The photon spectral distribution of the incident beam is an important aspect we had to take into account. To simulate an image, the photon spectrum has to be divided into a set of discrete energy values. Each energy value is associated with a photon number, which is a fraction of the total photon number of the whole spectrum. So far, we have used the catalogue of Birch et al. [7], in which semi-empirical spectral data, in the tube voltage range from 30 to 140 kV, are tabulated. For each energy value, the photon attenuation calculations have to be repeated. The corresponding attenuation coefficients, associated with any elementary or

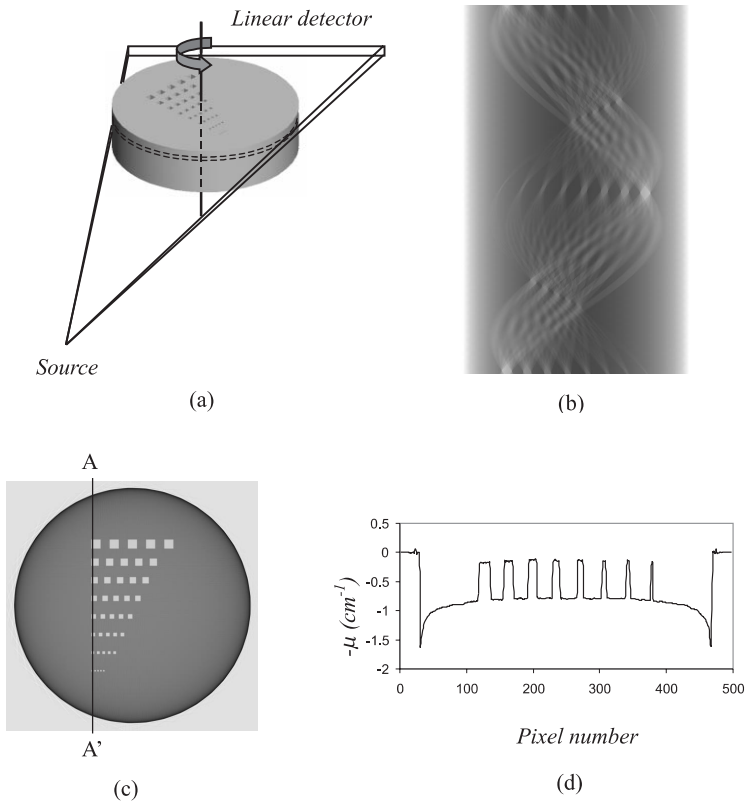

Fig. 7. Simulation of a tomographic slice on an aluminum spatial resolution phantom. (a) Schematic view of the simulated setup. (b) Simulated sinogram composed of 800 projections. (c) Reconstructed slice. (d) Profile of the reconstructed value of μ, corresponding to the line AA'. The baseline of the profile has a characteristic curved shape. This phenomenon, called "cupping effect", is due to the beam hardening.

compound substance, can be obtained by means of available databases, such as XGAM [8] or EPDL97 [9]. When performing a simulation, the detector is split into energy intervals (or channels) with an adjustable width, and a set of images associated with each one is stored. A global image, obtained by adding all those partial images, is also computed.

Thanks to the spectrum treatment, it is easy to monitor the spectrum evolution (beam hardening) when the beam goes through the object (Fig. 10). The influence of a filter, wherever it is located in the imaging chain, can also be studied easily. Simulation of dual energy imaging techniques can also be carried out. For example, we did a test with a cylindrical polyethylene sample, comprising two holes filled with water and a sodium iodide solution (Fig. 11). If we perform a "classic" image acquisition (with a polychromatic or monochromatic beam), it is very difficult to distinguish between water and the sodium iodide solution. To increase the contrast, we can take advantage of an absorption discontinuity of the iodine atoms, at 33.17 keV, that involves the electrons of the K shell. We simulated a "K-edge" image, by calculating the difference between two images, obtained with a monochromatic beam: the first one with an energy slightly lower than 33.17 keV and the second one with an energy slightly higher. The sodium iodide solution shows up clearly on the K-edge image. This technique, which can be implemented with filtered polychromatic beams, can be useful, for example, in the medical field [10]. Another kind of dual energy technique consists in acquiring data

at two energies sufficiently far apart for the attenuation at one energy to be due primarily to photoelectric interactions and the attenuation at the second energy to be due primarily to Compton scattering [11]. In all cases, simulation can be useful in calibrating the dual energy system under consideration and in testing its performance.

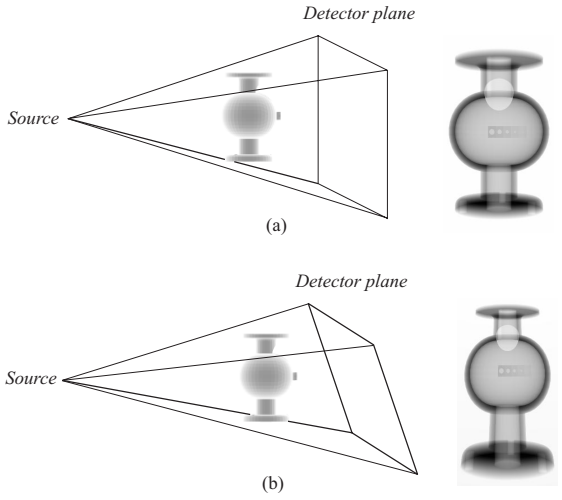

Fig. 8. Influence of the detector plane orientation on a radiographic image. (a) Simulated radiograph, with the detector plane perpendicular to the symmetry axis of the beam. (b) If the detector is tilted, different magnifications are obtained, depending on the part of the object we consider. In this example, the magnification is higher in the lower zone of the image.

4. Simulation algorithm

To summarize the points developed in the previous section and to give an overall view of our simulation code, we have represented its broad outline by means of a simplified diagram (Fig. 12). Before the beginning of the simulation, the whole virtual imaging chain has to be defined. Two databases are integrated in the software: the first one contains cross-sections and the second spectral data.

The simulation in itself consists of five loops that correspond to the incrementation of:

1. object positions, when several projections have to be computed (radioscopic or tomographic acquisition);
2. source points, when the source area is divided into elementary source points;
3. pixels of the detector;
4. energies of the spectrum;
5. distances covered in the object.

For each energy of the spectrum, a partial image, containing the number of photons associated with each pixel, is stored in a matrix. A global image is computed by calculating the total energy of the photons that reach each pixel of the detector.

By taking into account the iteration number in each loop, it is possible to predict how computation time evolves if more object movements, source points or pixels are necessary. Memory space also

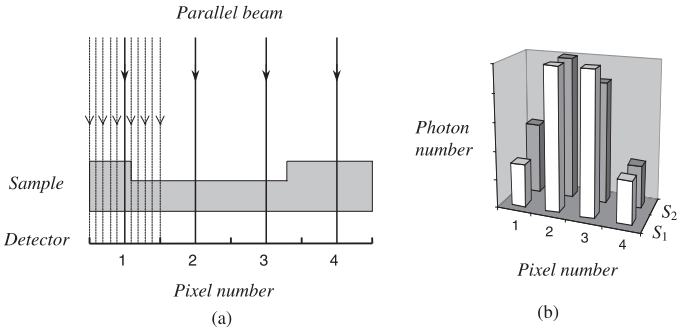

Fig. 9. Information losses may occur in the simulation process because discrete rays are used. (a) Schematic cross-section of an imaging setup, in a simple configuration (parallel beam). In a basic simulation, rays are traced towards the center of every pixel (thick rays). In reality, the whole surface of each pixel detects photons that have followed an infinity of different paths in the sample (thin rays). (b) Photon number histograms. In the basic simulation (histogram S_1), the calculated photon numbers corresponding to pixels 1 and 3 are biased. A more realistic calculation can be carried out by dividing each pixel into sub-pixels and by repeating ray-tracing for each of the latter. Therefore, every pixel simply gets the sum of all the photons detected by the sub-pixels (histogram S_2).

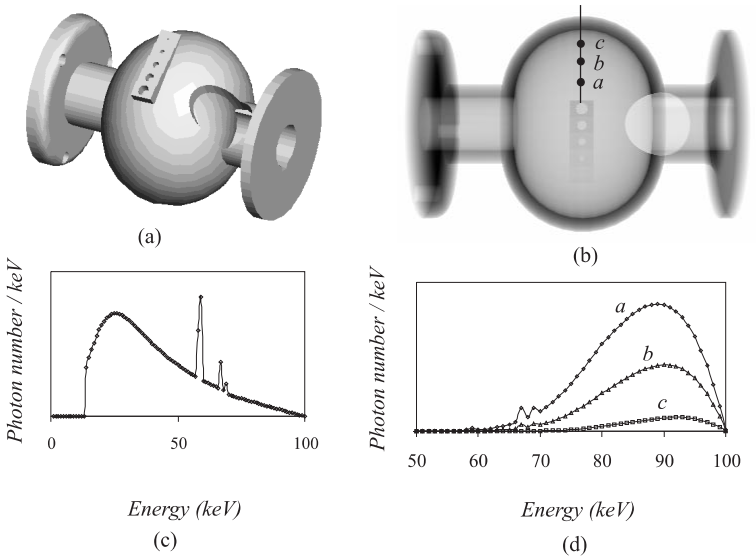

Fig. 10. Radiograph simulation of a gate, with a step wedge. A polychromatic beam (100 kV X-ray tube voltage) is used and the detector is split into 100 energy channels with a 1 keV interval. (a) CAD model of the gate. (b) Simulated radiograph. (c) Incident beam spectrum. (d) The transmitted photon spectra associated with the points labeled *a* to *c* reveal a beam hardening phenomenon, stronger where the part is thicker, i.e., close to the edge. The energy scales used to plot the incident and transmitted spectra are different.

has to be considered as a practical limit. Depending on the simulation type (simple radiographic projection, 2D tomographic slice, 3D tomography with a matrix detector), the computation time order of magnitude can vary from 0.1 s up to several hours on a PC, with a 400 MHz microprocessor.

5. Mapping of the contrast-to-noise ratio

5.1. Photon noise

5.1.1. Counting process of monochromatic photons: Poisson distribution

If we consider a monochromatic beam, all the photons play the same role and their detection is a counting process that obeys the Poisson distribution, noted $\mathscr{P}(\lambda)$, with the following probability distribution [12]:

$$p(x) = \frac{\lambda^x}{x!}\mathrm{e}^{-\lambda}, \quad x = 0, 1, 2, \ldots, \infty, \tag{4}$$

where $p(x)$ represents the probability of detecting x photons in a given time interval Δt, when λ is the expectation of the counting. The variance σ^2 of this distribution is just the mean value of the distribution

$$\sigma^2 = \lambda. \tag{5}$$

If the parameter λ is large enough ($\lambda > 20$), the Poisson distribution approximates to the normal distribution $\mathscr{N}(\lambda, \lambda)$ with both mean and variance equal to λ. The corresponding probability density function is given by

$$f(x) = \frac{1}{\sigma\sqrt{2\pi}}\mathrm{e}^{-[(x-\lambda)^2/2\sigma^2]}, \quad -\infty < x < +\infty. \tag{6}$$

5.1.2. Statistical distribution of the energy absorbed in the detector: case of a polychromatic beam

We assume that the detector absorbs the full energy of the photons that are transmitted through the sample and has a linear response. Thus, we can determine the theoretical statistical distribution of the signal (which is the total absorbed energy) associated with each pixel of the detector. As we have seen in the previous section in the case of a monochromatic beam, in each channel having the energy E_i, the photon number N_i detected in a

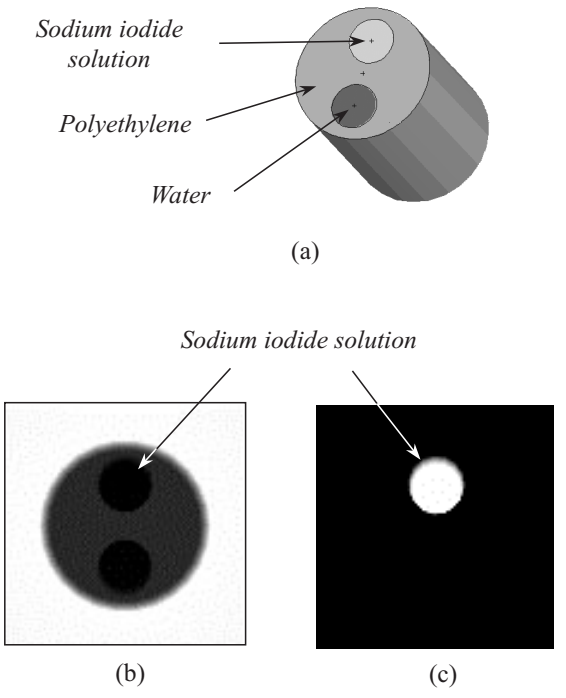

Fig. 11. Simulation of a K-edge image. (a) CAD model of the sample. (b) Simulated radiograph obtained with a monochromatic beam. In this classic image, the contrast between the two holes is very low. (c) A K-edge image was calculated by subtracting the first image, obtained with a monochromatic beam at 33.0 keV, from the second one, at 33.4 keV. The sodium iodide solution shows up clearly on this K-edge image.

counting experiment is the outcome of a random variable which obeys the Gaussian distribution $\mathcal{N}(\overline{N_i}, \overline{N_i})$. As Eq. (1) is completely deterministic, simulation gives straight $\overline{N_i}$. When using a polychromatic beam, the total absorbed energy derives from all the independent monochromatic photon distributions and it obeys the Gaussian distribution $\mathcal{N}(\sum_i E_i\overline{N_i}, \sum_i E_i^2\overline{N_i})$.

To simulate the influence of Gaussian noise on an image, we add to the energy value absorbed by each pixel a random number following the normal distribution $\mathcal{N}(0, \sum_i E_i^2\overline{N_i})$. If the absorbed energy is multiplied by a factor of k (for example, if we change the exposure time or the X-ray tube current), it is not necessary to carry out a new simulation, because the mean and the variance of the absorbed dose have simply to be multiplied by k. The signal-to-noise ratio

$$\mathrm{SNR} = \sum_i E_i\overline{N_i} \Big/ \sqrt{\sum_i E_i^2\overline{N_i}}$$

is then modified by a factor of $\sqrt{k}$. Fig. 13 presents an example of simulation with two different mean values of the absorbed energy. When the energy mean value decreases, the SNR clearly becomes less important.

5.2. Contrast-to-noise ratio

5.2.1. Definition

The SNR is a good parameter for quantifying the relative importance of the photon noise in an image. Nevertheless, it gives no indication about the detectability of any given defect in an object. Therefore, we need another quantitative parameter, called CNR, that takes into account both the photon noise and the contrast associated with the relevant defect. The contrast is the absolute value of the difference between the total absorbed energies calculated with and without the defect (suffixes A and B, respectively, in Eq. (7)). The noise is the standard deviation of the statistical distribution associated with the contrast. The CNR can thus be written as follows:

$$\mathrm{CNR} = \frac{\left|\left(\sum_i E_i\overline{N_i}\right)_A - \left(\sum_i E_i\overline{N_i}\right)_B\right|}{\sqrt{\left(\sum_i E_i^2\overline{N_i}\right)_A + \left(\sum_i E_i^2\overline{N_i}\right)_B}}. \tag{7}$$

We must emphasize the fact that CNR is associated with an individual pixel. In other words, it corresponds to a theoretical 1D defect placed on a single ray, with a thickness Δx and a material which have to be specified. The CNR parameter is therefore a quality indicator, which has a high value if the considered defect creates a contrast far higher than noise. In this case, the defect will be easy to detect.

The CNR is a relevant parameter mainly because it offers a means of determining the optimal experimental parameters (for example, tube voltage and various geometric parameters) to maximize the detection of defects. A systematic study of CNR maps versus various parameters is feasible by means of simulation, whereas such maps are impossible to obtain experimentally. Such a tool

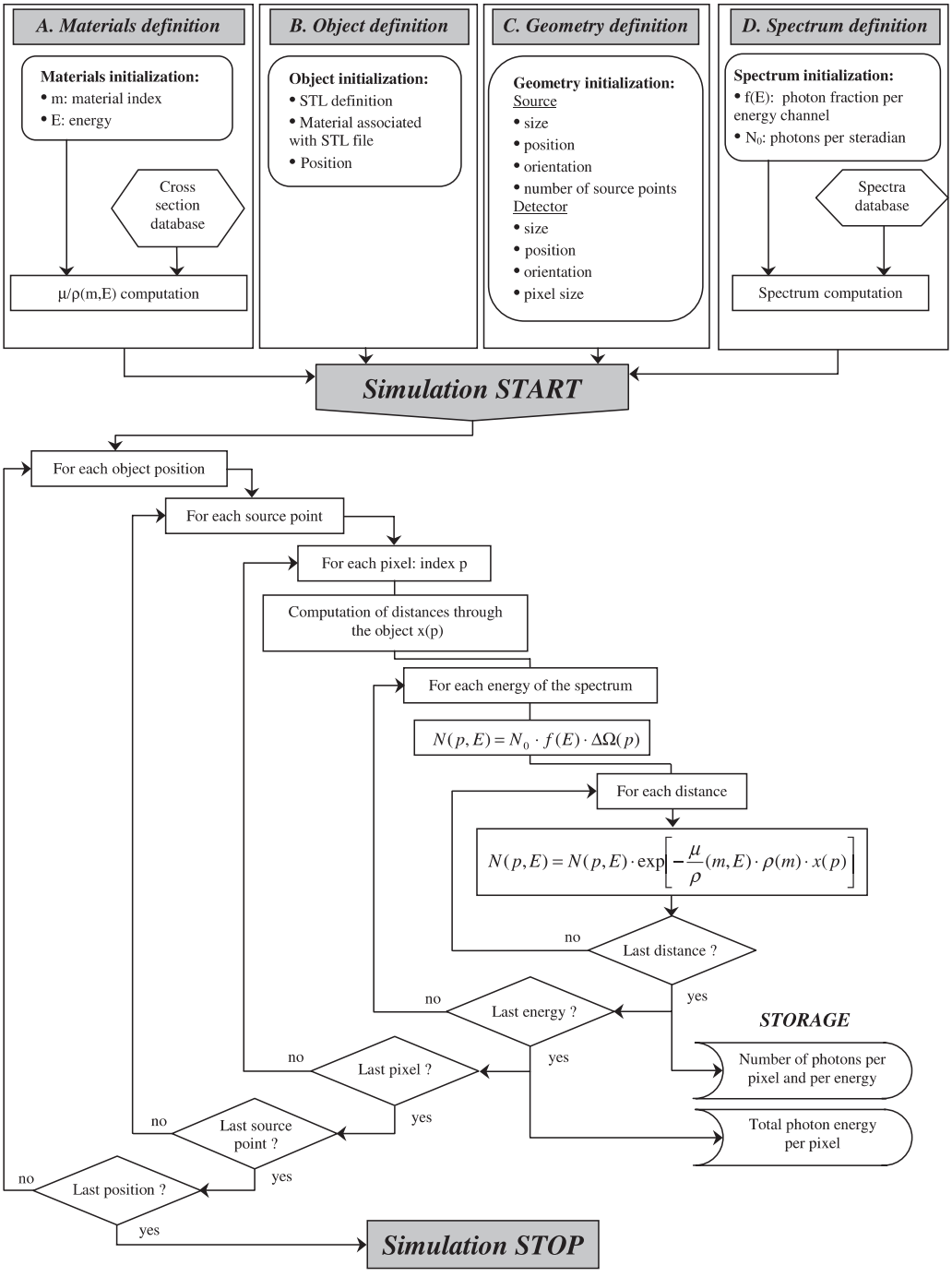

Fig. 12. Simplified diagram of the simulation algorithm. The simulation process consists of five loops that correspond to the incrementation of object positions, source points, pixels, energies of the spectrum and distances covered in the object.

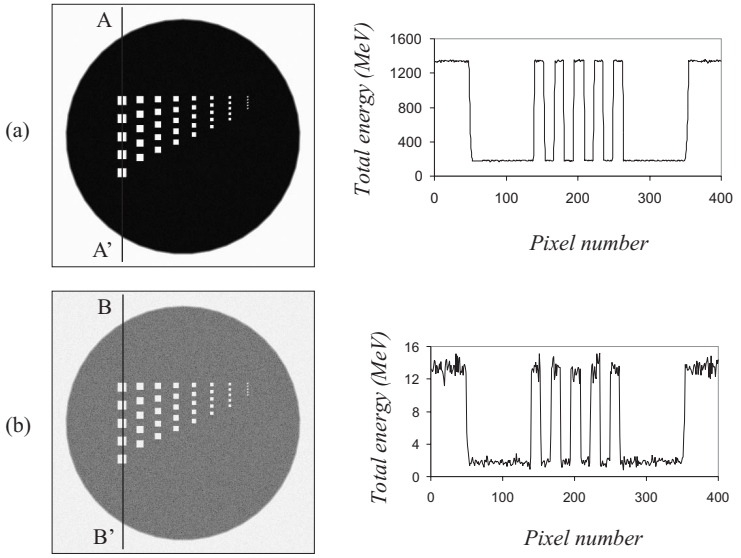

Fig. 13. Simulated radiographs of a spatial resolution phantom. The two images represent the total energy absorbed by a perfect detector (for this display, we took the logarithm of the total energy values and converted them into normalized gray levels). The total energy is 100 times higher in simulation (a) than in (b). The right part of the figure shows two profiles associated with lines (AA') and (BB'). It can be noticed that both the absolute noise and the signal-to-noise ratio increase with the total absorbed energy.

should result in considerable benefit, by reducing the number of experimental trials.

5.2.2. Application: weld testing by elliptic projection technique

As an example, we computed the CNR map corresponding to an elliptic projection of a welded joint between two cylindrical aluminum tubes. A radiograph simulation, without any defect in the object, was carried out. In parallel, we simulated a second image of the same welded joint, with 1 mm thick void defects placed in the path of every ray. These two images enabled a CNR map to be computed (Fig. 14). In this example, the CNR map clearly shows two dark zones, corresponding to high values of the distance covered in the object (close to the inner edge of the tube), where the detection of defects is difficult. To determine the optimal acquisition conditions, the percentage of the image surface (or possibly the percentage of the associated object volume), where CNR is lower than a given threshold, can be evaluated. The best acquisition parameters are the ones that minimize this percentage. For example, the optimal high voltage can thus be determined. Finally, it can be noticed that like SNR (see Section 5.1.2), if the exposure time or tube current is multiplied by a factor of k, CNR is multiplied by $\sqrt{k}$. Consequently, the CNR map does not have to be simulated again, when trying different noise levels.

6. Conclusions and future directions

This preliminary work phase enabled us to develop the framework of a computer code able to produce within a short time realistic synthetic images, simulating the operation of radiographic, radioscopic or tomographic devices. The strong points of this tool are the use of CAD models to describe complex 3D objects, the ability to adjust the geometry of every component of the imaging chain and to deal with a polychromatic beam. Initially, the computed images present no photon noise, but Gaussian random fluctuations can be added afterwards, if needed. Moreover, we can study the detectability of defects in the inspected part by computing the CNR, which can act as a

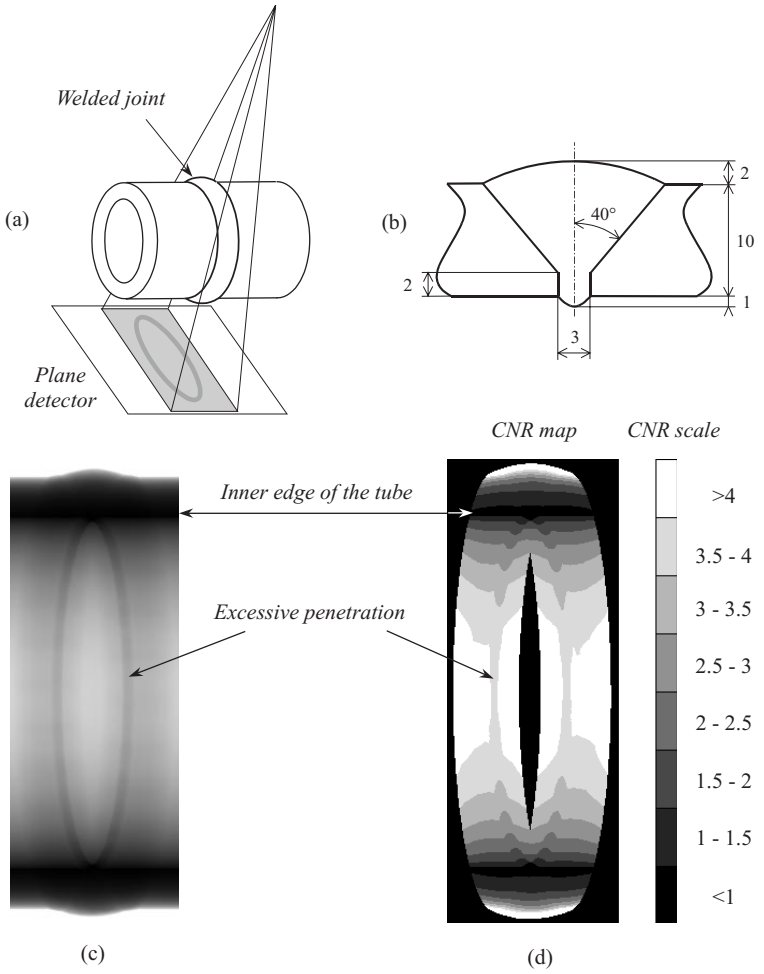

Fig. 14. Map of the CNR corresponding to an elliptic projection of a circular welded joint. (a) Schematic view of the setup configuration. (b) Schematic cross-section of the welded joint. Dimensions are indicated in millimeters. (c) Simulated radiograph obtained with a point source and a polychromatic beam (100 kV voltage). The excessive penetration of the welded joint is clearly visible (dark ellipse). (d) CNR map corresponding to a 1 mm thick void defect located in the welded joint. In the darkest areas of the map, CNR is very low and therefore defects will be very difficult to detect. The left and right-hand parts of the ellipse are slightly dissymmetric.

quantitative detectability indicator. CNR maps enable zones with low detectability to be identified, and, therefore, these maps can be useful in finding out the optimal acquisition parameters.

Several issues need further development and will be addressed in the next phase of our research program. As a priority, we are considering enriching our simulation tool by taking into account the scattering contribution. The 3D mapping of the absorbed dose in the sample will be broached simultaneously. Modeling and simulating the influence of the detector response on the image quality will also be an essential task. Finally, quantitative experimental validations will be necessary.

Possible application areas are numerous. Simulation can be useful when developing any specific NDT setup, in choosing the best components, optimizing the experimental parameters and saving time by reducing the number of experimental tests. Simulation also presents an important potential for testing the performance of

image-processing procedures in a virtual environment, where all parameters are fully controlled. It can also be used to interpret complex experimental data by comparing them to the corresponding simulation results [13]. In the foreseeable future, when simulation tools are widely used, NDT aspects will be taken into account more easily at the design stage. By simulating the inspection of a product, even before it is manufactured, it should be possible to avoid otherwise unexpected and tricky NDT problems afterwards.

References

[1] L.A. Feldkamp, S.A. Goldstein, A.M. Parfitt, G. Jesion, M. Kleerekoper, J. Bone Miner. Res. 1 (4) (1989) 3.
[2] G. Peix, J.Y. Buffiere, S. Cardinal, P. Cloetens, M. Salome, F. Peyrin, D. Babot, Caractérisation de l'endommagement dans les matériaux de structure par tomographie haute résolution à rayons X, Revue des composites et des matériaux avancés, Vol. 7, No. hors série, 1997, pp. 59–67.
[3] V. Kaftandjian, G. Peix, H. Bollon, P. Lion, in: Proceedings of the International Conference on Quality Control by Artificial Vision, QCAV'95, 1995, p. 202.
[4] F. Inanc, J.N. Gray, T. Jensen, J. Xu, in: Proceedings of the SPIE Conference on Physics of Medical Imaging, Vol. 3336, 1998, p. 830.
[5] P. Duvauchelle, G. Peix, D. Babot, NDT&E Int. 33 (2000) 23.
[6] P. Duvauchelle, N. Freud, V. Kaftandjian, G. Peix, D. Babot, in: J. Baruchel, J.-Y. Buffière, E. Maire, P. Merle, G. Peix (Eds.), X-ray Tomography in Material Science, Hermes, Paris, 2000, p. 127.
[7] R. Birch, M. Marshall, G.M. Ardran, Catalogue of Spectral Data For Diagnostic X-rays, The Hospital Physicists Association, 1979.
[8] M.J. Berger, NIST Standard Reference Database 8, X-ray and Gamma-ray Attenuation Coefficients and Cross Sections, XGAM, distributed by Office of Standard Reference Data, National Institute of Standards and Technology, Gaithersburg, MD 20899, 1988.
[9] D.E. Cullen, J.H. Hubbell, L. Kissel, EPDL97: The Evaluated Data Library, '97 Version, UCRL-ID-50400, Vol. 6, rev. 5, 1997.
[10] S.J. Riederer, C.A. Mistretta, Med. Phys. 4 (6) (1977) 474.
[11] P. Engler, W.D. Friedman, Mater. Eval. 48 (1990) 623.
[12] M.K. Ochi, Applied Probability and Stochastic Processes in Engineering and Physical Sciences, Wiley, New York, 1990.
[13] A. Koenig, A. Gliere, R. Sauze, P. Rizo, in: Proceedings of the Seventh European Conference on Non-destructive Testing, Vol. 1, 1998, p. 444.